의학박사 학위논문

In Vivo Cell Tracking After Subretinal Transplantation Using Magnetic Iron Oxide Labeling and Magnetic Resonance Imaging

망막하 공간 세포 이식 후 자성 산화철 나노입자 표지 및 자기공명영상을 이용한 생체 내 세포추적

2020년 2월

서울대학교 대학원

의학과 안과학전공

마 대 중

ABSTRACT

In Vivo Cell Tracking After Subretinal Transplantation Using Magnetic Iron Oxide Labeling and Magnetic Resonance Imaging

Dae Joong Ma

Department of Ophthalmology

College of Medicine

The Graduate School

Seoul National University

In vivo cell tracking is a powerful tool for the optimization and monitoring of cell therapy. Magnetic resonance imaging (MRI) can be used to visualize transplanted cells labeled with superparamagnetic iron oxide nanoparticles (SPIONs), as well as the surrounding tissues. However, the applicability of these techniques *in vivo* in the retina has not been investigated. The goal of this study was to evaluate the feasibility of SPION labeling and MRI tracking of cells which were transplanted into the subretinal space. Neuro-progenitor (NP) cells and photoreceptor precursors derived from human embryonic stem cells were labeled with SPIONs using the FeraTrack MRI contrast agent kit. SPION-labeled NP cells which were transplanted in the subretinal space of Brown-Norway rats were visualized with T2*-weighted sequences (T2*WI) MRI as hypointense signals for up to 20 weeks. The

proliferation, viability, and differentiation capacity of SPION-labeled photoreceptor precursors were assessed *in vitro* and were found to be unaffected by SPION labeling. Royal College of Surgeons (RCS) rats were classified into four experimental groups as follows: those injected with culture medium, unlabeled photoreceptor precursors, SPION-containing medium, and SPION-labeled photoreceptor precursors. All RCS rats underwent subretinal injection by a trans-scleral approach and were examined by MRI with T2*WI from 1 day to 12 weeks after transplantation. Hypointense signals corresponding to the transplanted SPION-labeled photoreceptor precursors and SPION-containing medium were clearly visible at the injection site at 1 day after transplantation. In contrast, no hypointense signal was observed in rats injected with culture medium or unlabeled photoreceptor precursors. The hypointense signal of the SPION-labeled photoreceptor precursors decreased but remained visible over the entire follow-up period. At 12 weeks after transplantation, histological analysis showed that transplanted SPION-labeled photoreceptor precursors were viable, and their distribution corresponded to the hypointense signal observed on T2*WI. However, the hypointense signal of the SPION-containing medium markedly decreased over time until it was undetectable at 12 weeks after transplantation. In addition, the SPION-labeled photoreceptor precursors showed similar therapeutic effect in RCS rats compared to the unlabeled photoreceptor precursors. This study demonstrated that the SPION labeling and MRI tracking of cells transplanted into the subretinal space is feasible and can be utilized in cell therapy for degenerative retinal diseases.

……

Keywords: Retina, Embryonic Stem Cells, Superparamagnetic Iron Oxide Nanoparticles, Photoreceptor Precursors, Magnetic resonance imaging

***Student Number*:** 2017-37618

CONTENTS

LIST OF TABLES AND FIGURES

Chapter 1

Chapter 2

LIST OF ABBREVIATIONS

RP, retinitis pigmentosa

AMD, age-related macular degeneration

RPE, retinal pigment epithelial

hESC, human embryonic stem cell

iPSC, induced pluripotent stem cell

MRI, magnetic resonance imaging

SPION, Superparamagnetic iron oxide nanoparticle

EB, embryoid body

SNM, spherical neural mass

BN rats, Brown-Norway rats

OCT, optical coherence tomography

ARPE-19, adult RPE-19

MTS, 3-(4, 5-dimethylthiazol-2-yl)-5 (3-carboxymethonyphenol)-2-(4-sulfophenyl)-2H-tetrazolium

TUNEL, terminal deoxyribonucleotidyl transferase (TDT)-mediated dUTP-digoxigenin nick end labeling

DAPI, 4', 6-diamidino-2-phenylindole

RT-PCR, real-time reverse transcription polymerase chain reaction

PDE6ß, phosphodiesterase 6 ß

GAPDH, glyceraldehyde-3-phosphate dehydrogenase

BSA, bovine serum albumin

PBS, phosphate-buffered saline

tuj1, Human neuronal class III te dehydro

RCS rats, Royal College of Surgeons rats

OKR, optokinetic response

c/d, cycles per degree

ERG, electroretinogram

GFP, green fluorescent protein

MSC, mesenchymal stem cell

GENERAL INTRODUCTION

Degenerative retinal diseases, such as retinitis pigmentosa (RP) and age-related macular degeneration (AMD), are a leading cause of incurable blindness worldwide. These degenerative retinal diseases are characterized by the loss of specific retinal cell types such as photoreceptors or retinal pigment epithelial (RPE) cells in the early stages, eventually leading to a profound loss of photoreceptors, which results in visual loss (1-3). Cell therapy might be a promising approach for preserving or restoring vision in advanced stages of degenerative retinal diseases, but obtaining the required cell types efficiently, in sufficient numbers, and in a timely manner remains a major challenge. Stem cells can serve as an unlimited source of appropriately differentiated cells for replacement. Landmark clinical trials of human embryonic stem cell (hESC)- or induced pluripotent stem cell (iPSC)-derived RPE cells transplanted into the subretinal space of patients with Stargardt disease or AMD have reported favorable safety and tolerability profiles (4, 5).

To improve the functional benefits of cell therapy, information on the long-term fate of transplanted cells, including their survival and biodistribution, is essential, as poor survival or misdistribution may be associated with suboptimal therapeutic outcomes (6, 7). Traditional histopathological analysis is not clinically applicable, as it does not provide longitudinal assessment of transplanted cells during the patient's

life. Therefore, in such cases, noninvasive *in vivo* cell tracking is an ideal methodology for evaluating cell distribution and fate (8).

Cellular magnetic resonance imaging (MRI), which aims at visualizing the cell in its entirety, has proven to be an effective technique for the noninvasive tracking of cellular therapeutics. Superparamagnetic iron oxide nanoparticles (SPIONs) have been widely used in cellular imaging and cell tracking studies involving MRI and are already FDA-approved for use in humans (8).

Although many studies have investigated the efficiency of imaging using MRI with SPIONs, no studies are available in the ophthalmologic field. The aim of this study was to determine the feasibility of SPION labeling and MRI as *in vivo* cell tracking after their subretinal transplantation.

CHAPTER 1

Magnetic Resonance Imaging Tracking of Magnetic Iron Oxide-Labeled Neuro-progenitor Cells after Subretinal Transplantation

INTRODUCTION

Subretinal injection is widely used in the treatment of degenerative retinal diseases, including cell therapy, gene therapy, and optogenetic therapy (9). The accurate delivery into the subretinal space is a key factor in these treatments.

The retina has a very thin but highly organized laminar structure with 10 distinct layers. A subretinal space is a potential space between the photoreceptor and RPE; an injection into this site produces a transient bleb (10). There are two possible approaches for subretinal injection: trans-vitreal and trans-scleral. The trans-vitreal approach can directly observe the needle end as it crosses the vitreous cavity and penetrates the retina to reach the subretinal space. However, the eyes of the young rodents, which are primarily used in experiments, are very small with the lens occupying a large volume. The trans-vitreal approach has a potential risk of lens damage in the eyes of small animals, which could result in the formation of cataract. This technique is more suitable for larger animals, including primates and humans.

In the trans-scleral approach, the needle penetrates the outer layers (sclera-choroid-RPE complex) of the eyeball, without damaging the retina. However, this technique is performed without direct observation of the needle end as it penetrates the sclera-choroid-RPE complex. Because the surface of the eye is curved, it is very hard to know the sufficient needle angles and depths for the subretinal injections. As a result, this technique has a long and steep learning curve, and has a high probability

of failure including breaching the retina and delivery of transplants into the vitreous cavity or choroid. In addition, since the choroid is a highly vascular tissue, the penetrating choroid has a high chance of causing subretinal hemorrhage. However, the trans-scleral approach does not involve the retina / vitreous and never touches the lens, which makes it more suitable for smaller animals, including rodents.

Creating a transient retinal bleb is generally used as an early indicator of a successful subretinal injection (6). However, a retinal bleb, which appears as pearlish white, is often difficult to notice in albino rodents that are widely used in research (11). In addition, a large volume of transplant is required to create an observable bleb, which is not always possible in the experiment settings. Therefore, a novel method for the early detection of the accurate subretinal injections, works with a small volume of transplant, and which can be applicable in the albino animals, is required.

MATERIALS AND METHODS

All procedures were approved by the institutional review board (IRB) of Seoul National University Hospital (SNUH) and the Institutional Animal Care and Use Committee (IACUC) of the Clinical Research Institute (CRI) at SNUH, and conducted in accordance with the Association for Research in Vision and Ophthalmology (ARVO) statement for the use of animals in ophthalmic and vision research.

Generation of neuro-progenitor cells and SPION labeling

Neuro-progenitor (NP) cells were derived from the hESC line SNUhES43. Differentiation of human hESCs to spherical neural masses (SNMs) followed Cho et al. with minor modifications (12). Colonies of undifferentiated hESCs were detached mechanically and cultured in a bacterial dish for 5 days to form embryoid bodies (EBs). EBs were cultured in NP selection medium for 5 days, and the NP cells were then expanded by continuously culturing the cells in expansion medium for 4 more days. Neural rosettes and neural tube-like structures observed during the neural expansion culture were mechanically isolated and cultured in NP expansion medium for another 7 days to form clumps of NP cells, i.e., SNMs.

NP cells were labeled with dextran-coated SPIONs (FeraTrack MRI contrast agent kit; Miltenyi Biotec Inc., Auburn, CA, USA) with an iron concentration of 100 μg/mL.

Cell transplantation

Five Brown-Norway (BN) rats (28 days old) were recruited for this exam. The rats were anesthetized with an intraperitoneal injection of a mixture of 10 mg/kg xylazine (Rompun; Bayer, Seoul, South Korea) and 20 mg/kg tiletamine/zolazepam (Zoletil 50; Virbac Laboratories, Carros, France). The corneas were anesthetized with a drop of 0.5% proparacaine hydrochloride (Paracaine; Hanmi Pharm, Seoul, South Korea), and the pupils were dilated with 0.5% tropicamide and 0.5% phenylephrine (Tropherine; Hanmi). Before injection of the cell suspension into the subretinal space, the cornea was punctured to reduce the intraocular pressure and to limit the efflux of injected cells.

After incision of the conjunctiva to expose the sclera, the sclera and choroid were penetrated with a 30-gauge syringe needle. Two microliters of medium or cell suspension (approximately 1×10^5 cells) was slowly injected into the subretinal space using a stainless-steel needle (33-gauge) connected to a Hamilton microsyringe (Hamilton, Reno, NV, USA) to produce retinal detachment in the superotemporal quadrant around the injection sites. The needle was kept in place for a few seconds

and then withdrawn very slowly to minimize the efflux of the injected cells. An immediate post-surgical fundus examination was performed to evaluate the quality of injections and monitoring for severe retinal damage or extensive hemorrhage. Rats with those signs were excluded from the study and euthanized.

To suppress immune activation, all animals were maintained on cyclosporine-A (Cipol N; Chong Kun Dang, Seoul, Korea) administered in the drinking water (210 mg/L) 1–2 days prior to the transplantation until they were euthanized (13).

Fundus photography and optical coherence tomography

The fundus photographs were taken using Optomap ultra-widefield imaging (Optos, Dunfermline, Scotland, UK) after anesthetization and pupillary dilation as described above. The optical coherence tomography (OCT) was taken using Spectralis spectral domain OCT (Heidelberg Engineering, Heidelberg, Germany).

Magnetic resonance imaging

All scanning was performed in a 9.4T MR scanner (Agilent 9.4T/160AS; Agilent Technologies, Santa Clara, CA, USA) using a Rapid 1H surface coil (RAPID Biomedical GmbH, Rimpar, Germany) for both radio-frequency transmission and

signal reception. During the scanning process, rats were anesthetized with 1.5% isoflurane. T2*-weighted MR images (T2*WI) were acquired with a gradient echo multi-slice sequence with 1.0 mm and 0.5 mm slice thickness.

Histology

The enucleated eyes were fixed with formalin for 48 h, embedded with paraffin, and cut on a microtome (Thermo Fisher Scientific, Walldorf, Germany) into 4-μm-thick sections. For Prussian blue staining, the sections were deparaffinized and stained with a Prussian blue staining kit (Polysciences, Inc., Warrington, PA, USA).

RESULT

Establishment of MRI protocol

T2*WI was acquired with two different protocols, using 1.0 mm and 0.5 mm slice thicknesses (Fig. 1). Four to five images with a high signal to noise ratio could be obtained for each eye with the 1.0 mm slice thickness protocol. However, the hypointense signal produced by SPION-labeled NP cells was missed or detected to be smaller in size, owing to the wide image section spacing (Fig. 1A). With the 0.5 mm slice thickness protocol, eight to nine images with a relatively low signal to noise ratio could be obtained for each eye. However, the hypointense signals produced by SPION-labeled NP cells were not missed in all eyes, owing to narrow image section spacing (Fig. 1B). The 0.5 mm slice thickness protocol was adopted in the subsequent study.

***Tracking of SPION-labeled neuro-progenitor cells* in vivo**

To evaluate the ability to track SPION-labeled NP cells *in vivo*, SPION-labeled NP cells were injected into the subretinal space of BN rats and imaged using MRI (Fig. 2). T2*WI clearly showed the location of the injected SPION-labeled NP cells as a hypointense signal over a period of 20 weeks.

The hypointense signal observed in T2*WI corresponded with the distribution of SPION-labeled NP cells, which were detected in histological sections as Prussian blue-stained areas in the subretinal space (Fig. 3).

In vivo ***cell tracking using fundus photography and optical coherence tomography***

Fundus photographs were taken at 4 days after transplantation (Figs. 4A and 4B). In both eyes, neurosensory retinal detachment with a clearly visible bleb was observed near the injection site. At 14 days after transplantation, the neurosensory retina was reattached and the blebs disappeared (Figs. 4C and 4D). No specific finding was observed near the injection site in OCT images. However, a hypointense signal in T2*WI was observed in one eye only (Fig. 4E); no hypointense signal was observed in the other eye (Fig. 4F).

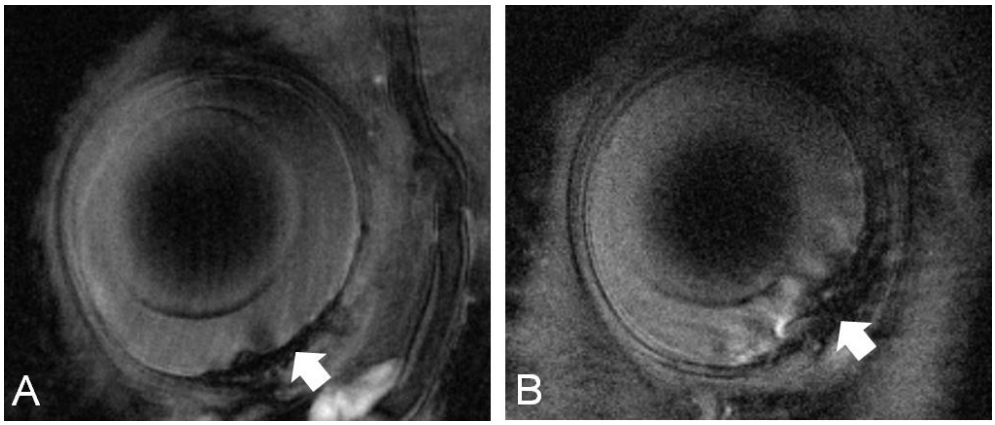

Figure 1. MRI images of SPION-labeled neuro-progenitor cells with different slice thickness protocols. (A) 1.0 mm slice thickness. (B) 0.5 mm slice thickness. The injected sites are marked with white arrows.

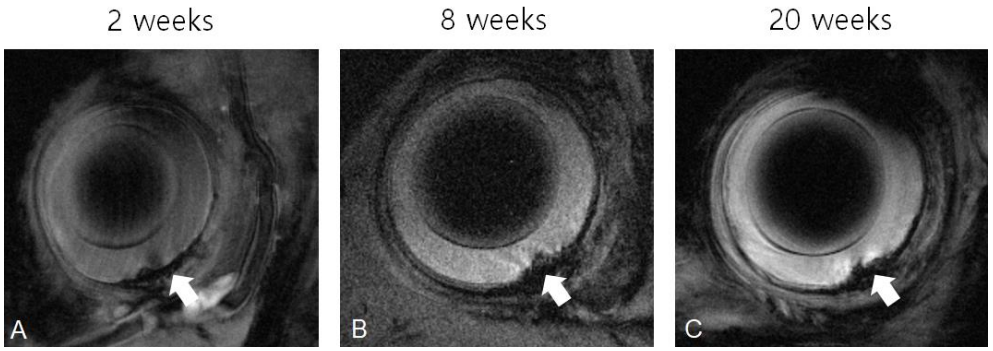

Figure 2. Tracking of transplanted SPION-labeled neuro-progenitor cells by MRI. Longitudinal T2*WI of Brown-Norway rats injected with SPION-labeled neuro-progenitor cells at (A) 2 weeks, (B) 8 weeks, (C) 20 weeks after transplantation. The injected sites are marked with white arrows.

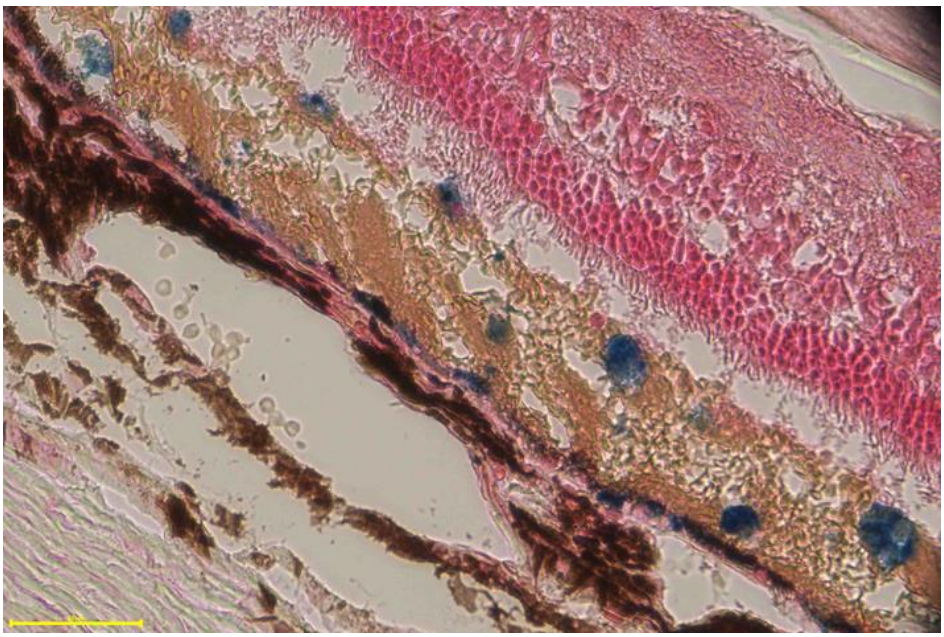

Figure 3. Histological analysis with Prussian blue staining of the transplanted SPION-labeled neuro-progenitor cells at 3 weeks after transplantation (bar = 50 μm).

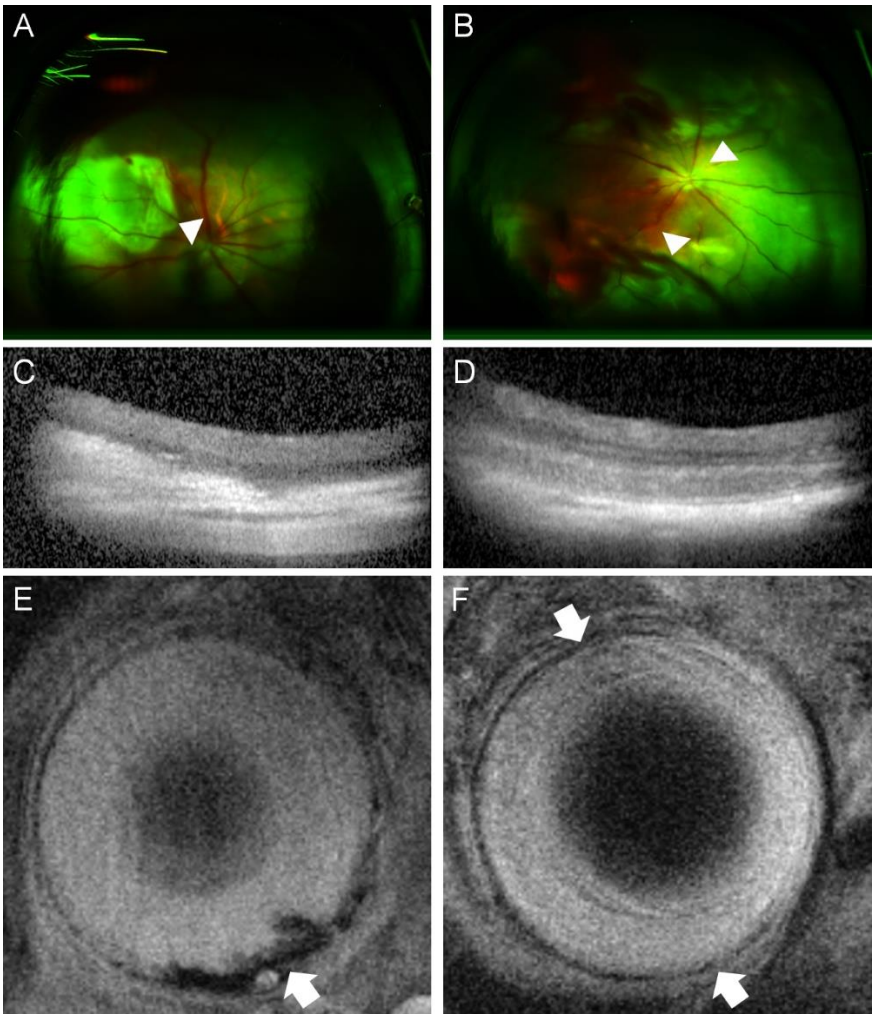

Figure 4. Fundus photo, optical coherence tomography, and T2*WI of SPION-labeled neuro-progenitor cells. Fundus photo at 4 days after transplantation (A, B). Optical coherence tomography at 2 weeks after transplantation (C, D). T2*WI at 2 weeks after transplantation (E, F). A, C, E, and B, D, F correspond to each rat, respectively. The margins of the retinal detachment are marked with arrowhead. The injected sites are marked with white arrows.

DISCUSSION

Traditionally, accurate cell delivery after subretinal transplantation was confirmed by the formation of a clearly visible retinal bleb (6). In this study, some eyes showed no hypointense signal in the T2*WI despite the initial retinal bleb formation (Figs 4B and 4F), which suggests that no SPION-labeled NP cell was residing in the subretinal space. The retinal bleb might be created mainly by the media injected during the subretinal injections, which occupied most of the volume of the transplant. Therefore, the initial retinal bleb formation does not guarantee accurate cell delivery into the subretinal space.

This study showed that SPION-labeled NP cells transplanted into the subretinal space and its surrounding tissues could be visualized with T2*WI for up to 20 weeks. This accurately indicated the presence and the location of the transplanted cells. T2*WI with 0.5 mm slice thickness was proven to be more suitable for tracking SPION-labeled NP cells in the subretinal space, considering the image section spacing, signal-to-noise ratio, and examination time. Using this novel technique, we could detect the inaccurate cell delivery in the case that showed the retinal bleb formation after the subretinal injection in the early period.

This study suggests that SPION labeling and MRI tracking are feasible for the *in vivo* tracking of cells transplanted into the subretinal space. However, further studies evaluating the effect of SPION labeling on the photoreceptor precursors or

RPE, including the proliferation, viability, differentiation capacity, and therapeutic efficacy, and long-term *in vivo* survival, are required for the clinical application of this novel *in vivo* cell tracking technique in the retinal cell therapy.

CHAPTER 2

Viability, Differentiation Capacity, Detectability, and Therapeutic Efficacy of Magnetic Iron Oxide-Labeled Photoreceptor Precursors for Magnetic Resonance Imaging

INTRODUCTION

Photoreceptors are the main light-sensing cells in the retina. Dysfunction and loss of photoreceptors are the major causes for degenerative retinal diseases, which eventually result in blindness. There are various options (such as optogenetic therapy, retinal prostheses, and cell therapy) considered for the treatment of degenerative retinal diseases but only few are expected to be effective in the late-stage of the disease. Among these, cell therapy is a promising strategy for late-stage degenerative retinal diseases. It could replace the cells that have already degenerated and preserve or restore vision.

Landmark clinical trials reported the safety and efficacy of pluripotent stem cell-derived RPE cells for the treatment of AMD and Stargardt disease (4, 5). However, since RPE is not a light-sensitive, RPE transplantation can be expected to have therapeutic efficacy in certain conditions only, primary RPE dysfunction or degeneration, or where there is a photoreceptor abnormality secondary to an RPE defect, but not in the end-stage disease conditions with severe photoreceptor loss.

Photoreceptor transplantation can exhibit therapeutic effects in early and advanced degenerative retinal diseases through the following mechanisms: transplanted photoreceptors remain in the subretinal space and engage in cytoplasmic material transfer to the host photoreceptors; transplanted photoreceptors migrate into the host retina and form synapses with host cells such as remnant photoreceptors or

second order neurons, i.e. bipolar and/or horizontal cells (14). However, these mechanisms are thought to have a therapeutic effect in regions near the transplanted cells only, indicating that the information of the survival and biodistribution of transplanted cells is essential to improve the therapeutic efficacy of cell therapy.

In our previous study, SPION labeling and MRI tracking were found to be feasible for the *in vivo* tracking of the cells transplanted into the subretinal space. However, the effects of SPION labeling on the photoreceptor precursors have not been evaluated. These effects are essential for the clinical application of this technique in retinal cell therapy. Hence**,** the aim of this study was to determine the effects of SPION labeling on the proliferation, viability, differentiation capacity, therapeutic efficacy, long-term *in vivo* survival, and detectability on MRI of photoreceptor precursors.

MATERIALS AND METHODS

All procedures were approved by the IRB of SNUH and the IACUC of the CRI at SNUH, and conducted in accordance with the ARVO statement for the use of animals in ophthalmic and vision research.

Generation of photoreceptor precursors

NP cells were derived from hESCs as described above. Neural rosettes and neural tube-like structures observed during the neural expansion culture were mechanically isolated and cultured in NP expansion medium for another 7 days to form clumps of NP cells, i.e., SNMs. For passaging, the SNMs were mechanically fragmented into 4–6 pieces and expanded for 7–10 days. During passages 1–4, some SNMs containing opened neural tube-like structures or cystic structures were removed. SNMs at passages 3–8 were mechanically cut into small-sized fragments and enzymatically dissociated into single cells. Single cells were transferred onto a culture dish and maintained in suspension culture to reform SNMs over 5–7 days. For photoreceptor precursor differentiation, a non-contact co-culture system with adult RPE-19 (ARPE-19) cells (ATCC, Manassas, VA, USA) was used. Reformed SNMs were dissociated into single cells and re-seeded on cell culture inserts coated with CELLstart CTS (Gibco). ARPE-19 cells were seeded on the bottom of the CELLstart CTS-coated culture plates. After a day, these two types of cells were cultured together

for 7 days in a differentiation medium containing 1% N2 supplement CTS and 1% B27 supplement CTS (Gibco). Culture medium was changed every other day during the differentiation period (Fig. 5).

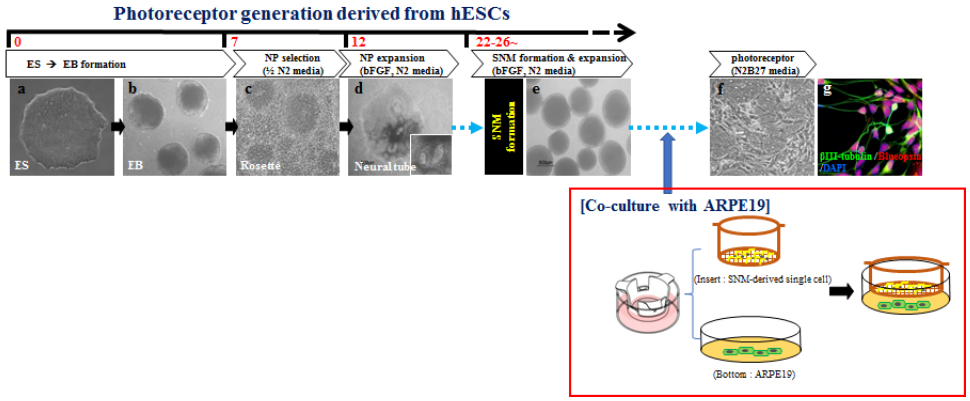

Figure 5. Schematic diagram of differentiation of human embryonic stem cells into photoreceptor precursor cells. It usually takes about 14 days to generate photoreceptor precursors from spherical neural masses (SNMs). After serial differentiation of human embryonic stem cells into SNMs, the non-cystic SNMs differentiated into photoreceptor precursor cells.

ARPE, human adult retinal pigment epithelial cell

SPION labeling

For cell labeling, photoreceptor precursors at passages 3–5 were incubated in medium supplemented with dextran-coated SPIONs (FeraTrack MRI contrast agent kit; Miltenyi Biotec Inc.) with an iron concentration of 100 μg/mL. The labeling medium was removed after 4–6 h cultivation.

Prussian blue staining

A Prussian blue staining kit (Polysciences) was used to determine the efficiency of SPION labeling. Unlabeled and SPION-labeled photoreceptor precursors were fixed with 4% paraformaldehyde (Affymetrix. Inc., Cleveland, OH, USA) for 15 min, washed three times with phosphate-buffered saline (PBS; Gibco), incubated with 4% potassium ferrocyanide in 4% hydrochloride solution for 30 min, washed again, and counterstained with nuclear fast red (Sigma-Aldrich, St. Louis, MO, USA).

MTS assay

The cell proliferation of unlabeled and SPION-labeled photoreceptor precursors was assayed using the MTS assay. MTS/PMS solution (containing CellTiter 96 AQ_{ueous} MTS reagent powder [Promega, Madison, WI, USA] and PMS

[Sigma-Aldrich]) was added to cultured cells and incubated at 37℃ in a 5% CO_2 incubator for 4 h. Absorbance was recorded at 490 nm with a VERSAmax microplate reader (Molecular Devices, Sunnyvale, CA, USA).

TUNEL analysis

The TUNEL assay was performed to identify the apoptosis of unlabeled and SPION-labeled photoreceptor precursors using a Click-iT TUNEL Alexa Flour imaging assay kit (Invitrogen, Carlsbad, CA, USA) at 1 day and 3 weeks after labeling, followed by counterstaining with DAPI (Molecular Probes, Eugene, OR, USA). TUNEL-positive cells were detected and counted using an Optinity KI-2000F fluorescence inverted microscope (Korea Lab Tech, Gyeonggi, Korea).

Quantitative RT-PCR

Total RNA from unlabeled and SPION-labeled photoreceptor precursors was isolated using the TRIzol LS reagent (Invitrogen), and cDNA was synthesized using the Superscript kit (Invitrogen). RT-PCR was performed on a CFX96 real-time system using the iQ SYBR Green Supermix (Bio-Rad, Hercules, CA, USA) according to the manufacturer's protocol the following transcripts: S-opsin, L-opsin, PDE6ß, recoverin, and rhodopsin. The primers are listed in Table 1.

Table 1. Primer sequences.

Genes	***Primer sequences (5'–3')***
S-opsin	F-TACCTGGACCATTGGTATTGGCGT R-TAAGTCCAGCCCATGGTTACGGTT
L-opsin	F-GCATCCGTCTTCACAAATGG R-CACAGCAGACCAGATCCAGG
PDE6ß	F-ATGCCCATCGTCAACAAGAA R-GCTCCTCCTTCAGGATTTCG
Recoverin	F-CCAAGTTCTCGGAGGAGGAG R-ATCTTCTCGGCTCGCTTTTC
Rhodopsin	F-CACAGGATGCAATTTGGAGG R-CCTTCTGTGTGGTGGCTGAC
GAPDH	F- ACCACAGTCCATGCCATCAC R-TCCACCACCCTGTTGCTGTA

GAPDH, glyceraldehyde-3-phosphate dehydrogenase

Immunofluorescence

After unlabeled and SPION-labeled photoreceptor precursors were fixed in 4% paraformaldehyde for 15 min, they were permeabilized in 0.3% Triton X-100 (Sigma-Aldrich) for 5 min and blocked with 3% bovine serum albumin (BSA) solution in PBS containing 0.3% Triton X-100 for 1 h. The antibodies used are listed in Table 2. Cell nuclei were counterstained with DAPI (Molecular Probes).

Flow cytometry analysis

Unlabeled and SPION-labeled photoreceptor precursors at passages 3–5 were split and incubated until confluence before flow cytometry analysis. Cultivated photoreceptor precursors were fixed with 2% formaldehyde for 10 min, blocked with human Fc blocker (BD Bioscience, Piscataway, NJ, USA) for 10 min, and permeabilized in 0.05% Triton X-100 for 15 min. The antibodies used are listed in Table 2. Cell fluorescence was measured using the Attune NxT acoustic focusing cytometer (Thermo Fisher Scientific, Waltham, MA, USA), and data were analyzed using Attune NxT software (Thermo Fisher Scientific).

Table 2. List of antibodies used

	Antibody name	Company	Host species	Dilution	Application
Primary antibody	Human neuronal class III β-tubulin (tuj1)	BioLegend	Mouse	1:500	IF, FCM, histology
	Human nuclei	Millipore	Mouse	1:50	IF
	Human mitochondria	Millipore	Mouse	1:100	IF
	Human rhodopsin	Millipore	Rabbit	1:100	IF, histology
	PDE6β	Abcam	Rabbit	1:50	IF
				1:100	FCM, histology
	L-opsin	Chemicon	Rabbit	1:100	IF, FCM, histology
	Recoverin	Chemicon	Rabbit	1:100	IF, histology
	S-opsin	Chemicon	Rabbit	1:100	FCM
Secondary antibody	Anti-mouse Alexa Fluor 488	Molecular Probes	Mouse	1:200	IF, FCM, histology
	Anti-rabbit Alexa Fluor 594	Molecular Probes	Rabbit	1:200	IF, FCM, histology

IF, Immunofluorescence; FCM, flow cytometry

Cell transplantation

Seventy Royal College of Surgeons (RCS) rats (21 days old) were randomly assigned to one of four groups: medium group (rats injected with culture medium, n = 15), photoreceptor precursor group (rats injected with unlabeled photoreceptor precursors, n = 11), SPION-medium group (rats injected with SPION-containing culture medium, n = 28), and SPION-photoreceptor precursor group (rats injected with SPION-labeled photoreceptor precursors, n = 16). The cell transplantation procedure was performed as described above.

Histology

The enucleated eyes were fixed with formalin, embedded with paraffin, cut on a microtome, and stained with Prussian blue as described above. For immunostaining, the sections were deparaffinized, exposed to target retrieval solution (DaKo, Santa Clara, CA, USA) at 95℃ for 20–30 min, and blocked with 3% BSA and 0.3% Triton X-100 for 1 h.

The antibodies used are listed in Table 2. Cell nuclei were counterstained with DAPI (Molecular Probes). The distribution area of the transplanted cells in histological sections was measured by ImageJ software (National Institutes of Health, Bethesda, MD, USA).

Magnetic resonance imaging

Four rats from each group were subjected to MRI analysis at 1 day and 12 weeks after transplantation. Additional follow-ups with MRI were performed for the rats in the SPION-medium group and SPION-photoreceptor precursor group at 2, 4, and 8 weeks after transplantation. All scanning was performed with the same MR scanner used in the prior study after being anesthetized with 1.5% isoflurane. T2*WI were acquired with a gradient echo multi-slice sequence using the following sequence parameters: repetition time, 2,000 ms; echo time, 9.26 ms; flip angle, 20°; average, 1; matrix, 512 × 512; field of view, 25.0 × 25.0 mm^2; slice thickness, 0.5 mm; and scan time, 17 min 8 s. For whole body imaging, the body was divided into three zones and scanned separately.

The proportion of the hypointense signal area was calculated as the hypointense signal area divided by the cross-sectional area of the eyeball in T2*WI, which was measured by ImageJ software.

Optokinetic response

Visual acuity was measured using optokinetic response (OKR) were recorded in each rat at 2, 4, 8, and 12 weeks after transplantation with an in-house testing apparatus. The in-house testing apparatus consists of a rotating drum with alternating high-contrast stripes (black and white) of different spatial frequencies (0.03, 0.05, 0.1, 0.15, 0.2, 0.25, 0.3, 0.4 and 0.5 cycles per degree [c/d]).

Each rat was placed on the platform in a quiet environment before the test until it became accustomed to the test conditions with minimal movement. The rat is placed in a clear plastic stationary round chamber at the center of the drum, which allows visualization and exposure of only one eye to the stimulus. The drum was rotated counterclockwise for the right eyes and clockwise for the left eyes. A video camera situated above the rat records the rat's head movements during one minute for later analysis and scoring by c/d. Head turn was scored only when the speed of tracking corresponded to the speed of the rotation of the stripes. Habitual and other random head movements were excluded when computing the score.

Electroretinogram recording

Full-field electroretinograms (ERGs) were recorded in each rat at 2, 4, 8, and 12 weeks after transplantation. Animals were dark-adapted over 6 h. After being anesthetized, the eyes were dilated and topically anesthetized in the same manner as for the transplantation. Each rat was laid prone with its face fully placed in the light stimulus dome of a Handheld Multispecies electroretinogram unit (HMsERG system; Ocuscience LLC, Henderson, NV, USA). A rodent contact lens with a silver-embedded thread electrode (Ocuscience LLC) was placed directly on the cornea after the application of 2% hydroxypropyl methylcellulose gel (Hycell solution; Samil Pharm Co., Ltd., Seoul, Korea). Subcutaneous needle electrodes in the forehead and thigh served as the reference and ground electrodes. Scotopic flash series were

recorded with a light flash intensity of 10 cd ・ s/m^2. The data were analyzed using ERGVIEW (Ocuscience LLC). The b-wave amplitude determined from the trough of the a-wave to the peak of the b-wave was analyzed.

Statistical analysis

Data are presented as the means ± standard deviations. The Mann–Whitney *U*-test was used to test the significance of comparisons among groups. A bivariate relationship between the hypointense signal region area in the T2*WI and the distribution area of the transplanted cells in the histological sections was examined using the Pearson product-moment correlation coefficient test. Statistical analysis was performed using SPSS version 22.0 (IBM, Armonk, NY, USA); differences with $p < 0.05$ were regarded as statistically significant.

RESULTS

SPION labeling of photoreceptor precursors

Unlabeled and SPION-labeled photoreceptor precursors were stained with Prussian blue for iron oxides. Compared to the unlabeled controls (Fig. 6A), SPION-labeled photoreceptor precursors displayed strong blue staining at 1 day after labeling, expressing abundant intracytoplasmic blue inclusions (Fig. 6C). At 3 weeks after labeling, SPION-labeled photoreceptor precursors still stained positive for iron oxides but in a more diluted fashion (Fig. 6D). There was no morphological change after SPION labeling compared to the unlabeled controls (Fig. 6A and 6B).

Viability and proliferation of SPION-labeled photoreceptor precursors

Possible cytotoxicity of SPION labeling on photoreceptor precursors was evaluated by TUNEL assay at 1 day and 3 weeks after labeling. Cell viability was not affected by the presence of SPION. TUNEL-positive cells accounted for 7.4% ± 0.5% of SPION-labeled cells compared with 6.5% ± 0.7% of unlabeled controls at 1 day after labeling (Fig. 7A and 7B) and 12.5% ± 0.7% of SPION-labeled cells compared with 11.0% ± 1.1% of unlabeled controls at 3 weeks after labeling (Fig. 7C and 7D).

Cell proliferation was not largely affected by the presence of SPIONs, as MTS assays showed that the proliferation rate was 90.0% ± 9.6% in SPION-labeled

cells compared with 100.0% ± 6.7% in unlabeled controls at 1 day after labeling (Fig. 8A) and 92.0% ± 3.6% in SPION-labeled cells compared with 100.0% ± 2.5% in unlabeled controls at 3 weeks after labeling (Fig. 8B).

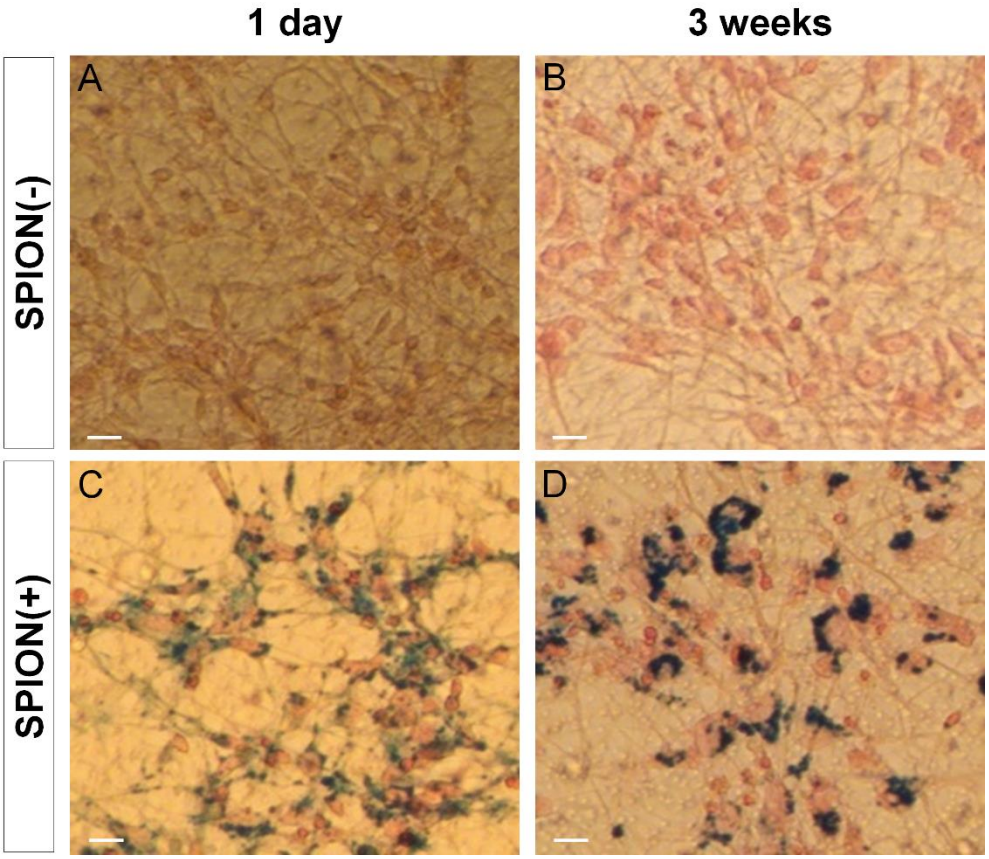

Figure 6. Prussian blue staining for SPION uptake. Unlabeled and SPION-labeled photoreceptor precursors were stained with Prussian blue at 1 day (unlabeled: A, SPION-labeled: C) and 3 weeks (unlabeled: B, SPION-labeled: D) after labeling (bar = 20 μm).

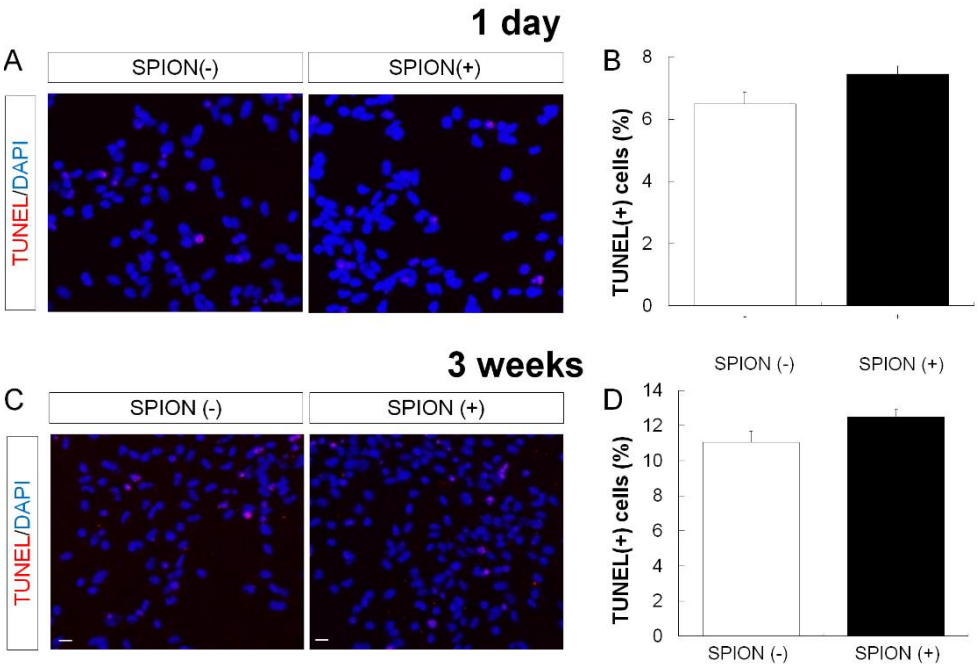

Figure 7. TUNEL analysis for cell viability. The cell viability of unlabeled controls and SPION-labeled photoreceptor precursors was evaluated at 1 day and 3 weeks after labeling by fluoromicrography (A: 1 day, C: 3 weeks). The percentage of TUNEL-positive cells was also determined at 1 day and 3 weeks after labeling (B: 1 day, D: 3 weeks) (bar = 20 μm). Error bars indicate standard deviations.

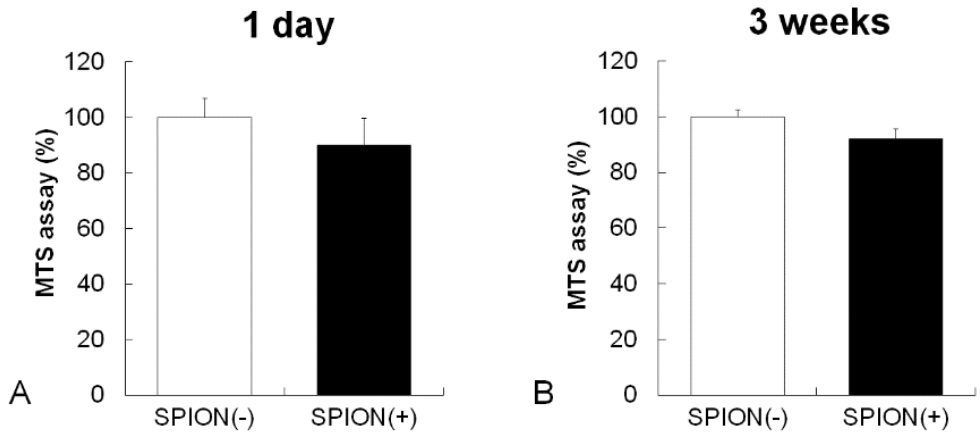

Figure 8. MTS assay for cell proliferation. The proliferation rates of unlabeled controls and SPION-labeled photoreceptor precursors were evaluated at 1 day (A) and 3 weeks (B) after labeling. Error bars indicate standard deviations.

Differentiation capacity of SPION-labeled photoreceptor precursors

To confirm the photoreceptor phenotype of the photoreceptor precursors, quantitative RT-PCR, immunofluorescence, and flow cytometry analysis were performed to assess the expression of photoreceptor-specific markers. In quantitative RT-PCR, the expression levels of the photoreceptor-specific mRNA were similar between unlabeled and SPION-labeled photoreceptor precursors at 1 day and 3 weeks after labeling (Fig. 9A and 9B, respectively). Similarly, immunocytochemical staining for human rhodopsin, PDE6ß, recoverin, and L-opsin showed similar expression levels in both unlabeled and SPION-labeled photoreceptor precursors at 1 day and 3 weeks after labeling (Fig. 10A and 10B, respectively). Fluorescence-activated cell sorting showed that all investigated markers, including TuJ1, L-opsin, PDE6ß, and S-opsin, were highly expressed at 1 day and 3 weeks after labeling and were present at similar levels between unlabeled and SPION-labeled photoreceptor precursors (Fig. 11A and 11B, respectively).

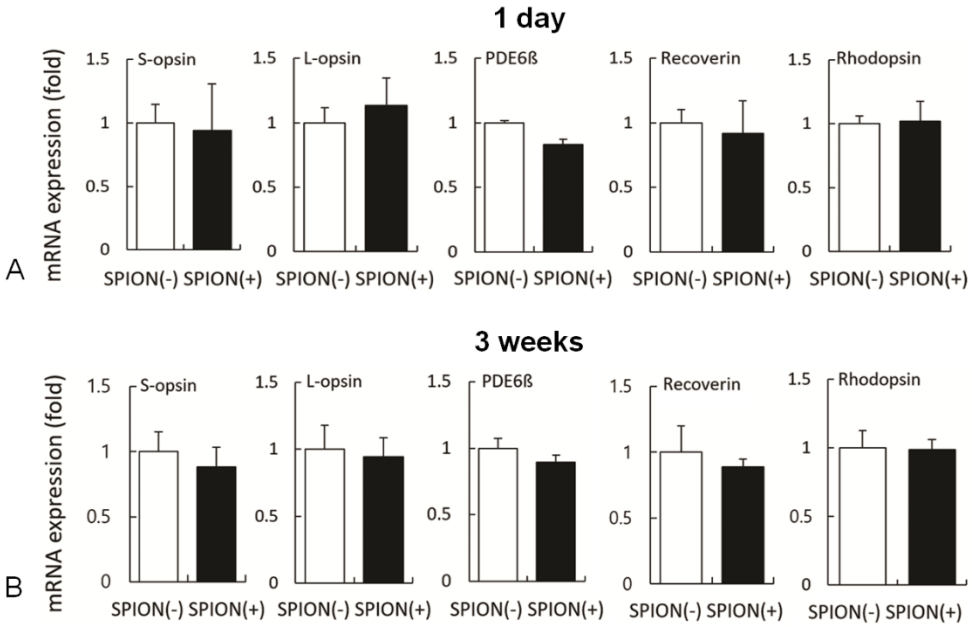

Figure 9. Analysis of photoreceptor-specific mRNA expression of photoreceptor precursors using quantitative RT-PCR. Photoreceptor-specific mRNA expression of unlabeled and SPION-labeled photoreceptor precursors was evaluated using quantitative RT-PCR at (A) 1 day and (B) 3 weeks after labeling. Error bars indicate standard deviations.

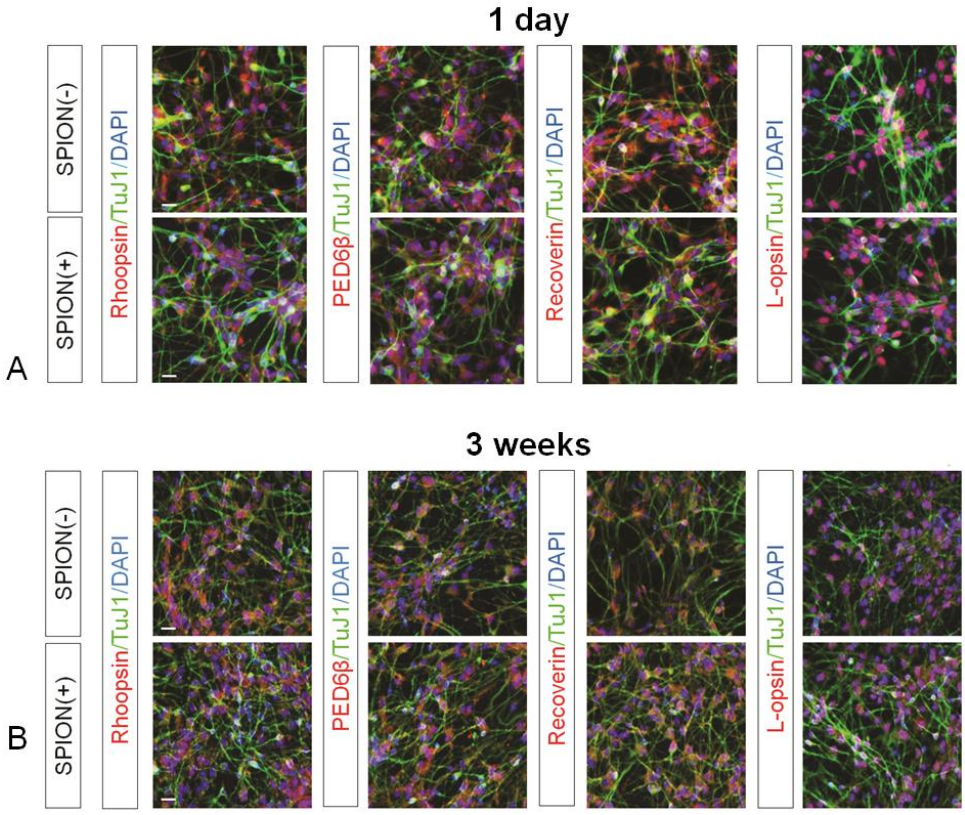

Figure 10. Analysis of photoreceptor-specific protein expression of photoreceptor precursors using immunostaining. Photoreceptor-specific protein expression of unlabeled and SPION-labeled photoreceptor precursors was evaluated at 1 day and 3 weeks after labeling using immunostaining at (A) 1 day and (B) 3 weeks after labeling (bar = 20 μm).

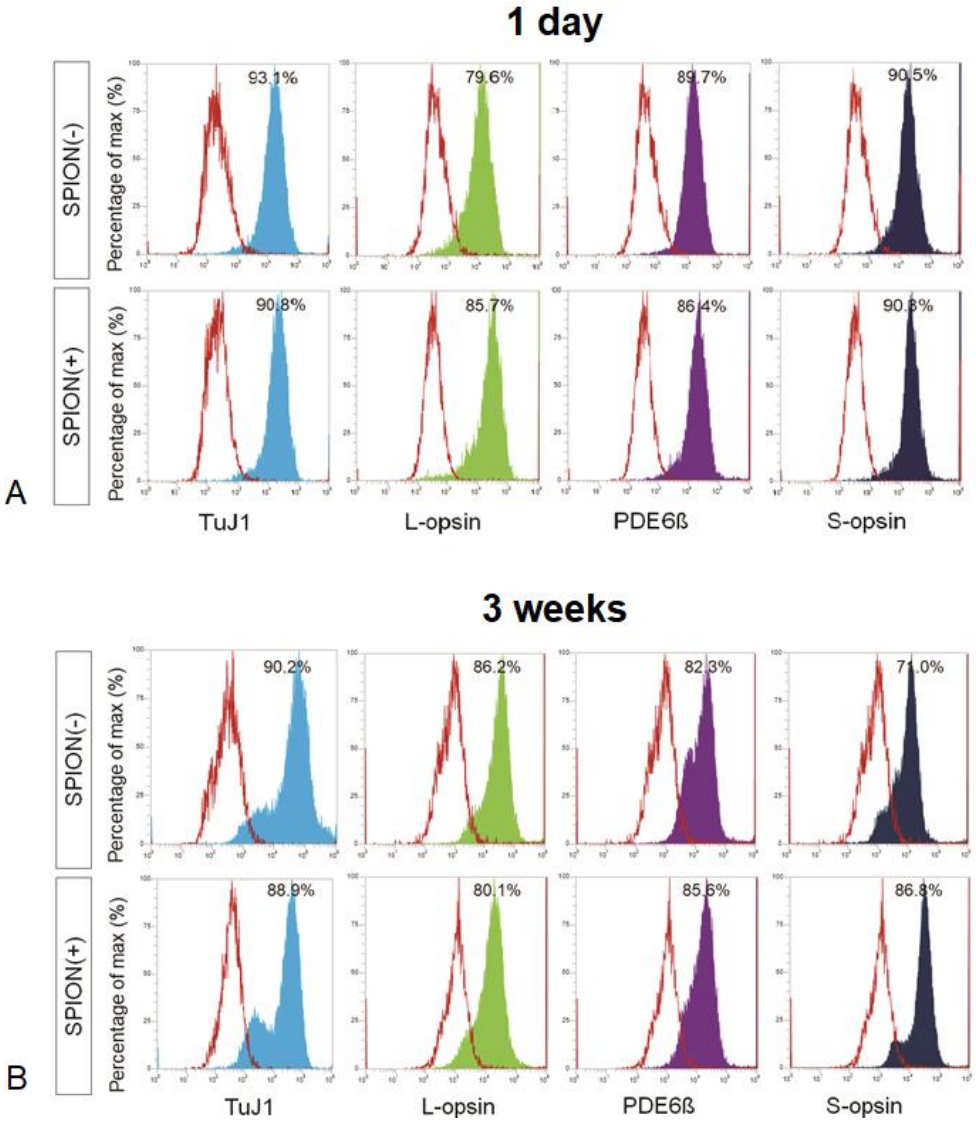

Figure 11. Analysis of photoreceptor-specific protein expression of photoreceptor precursors using FACS. Photoreceptor-specific protein expression of unlabeled and SPION-labeled photoreceptor precursors was evaluated at 1 day and 3 weeks after labeling using FACS at (A) 1 day and (B) 3 weeks after labeling.

***Tracking of photoreceptor precursors* in vivo**

To evaluate the ability to track SPION-labeled photoreceptor precursors in an *in vivo* environment, the culture medium, SPION-containing culture medium, unlabeled photoreceptor precursors, and SPION-labeled photoreceptor precursors were injected into the subretinal space of RCS rats and imaged by MRI (Fig. 12). T2*WI clearly showed the location of the injected SPION-labeled photoreceptor precursors as a hypointense signal over a period of 12 weeks (Fig. 12A). While the size of the hypointense signal on T2*WI gradually decreased, it remained present until 12 weeks after transplantation. The location of the SPION-containing medium was clearly visible, appearing as a hypointense signal on T2*WI at 1 day after transplantation. However, it was markedly reduced in size at 2 weeks, gradually decreasing until it was undetectable at 12 weeks after transplantation (Fig. 12B). In contrast, T2*WI could not clearly show the position of the unlabeled photoreceptor precursors (Fig. 12C) or medium (Fig. 12D) in the subretinal space at 1 day and 12 weeks after transplantation.

The hypointense signal observed in T2*WI (Fig. 13B–13D) corresponded with the distribution of the SPION-labeled photoreceptor precursors, which was detected in histological sections as Prussian blue-positive areas in the subretinal space (Fig. 13A).

In the whole-body imaging, the hypointense signal of the SPION-labeled photoreceptor precursors was indistinguishable from the hypointense signal of the internal organs (Fig. 14).

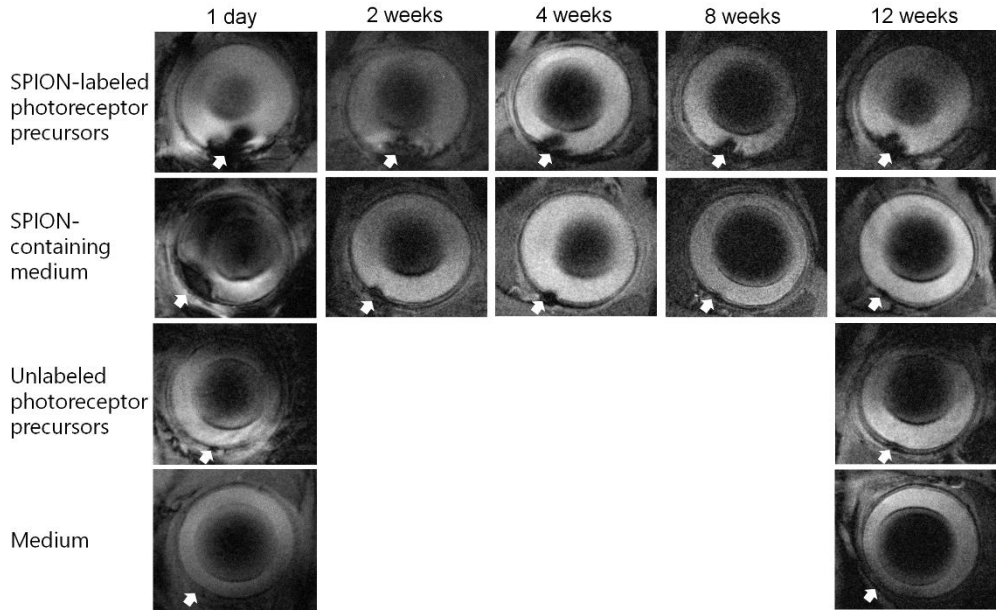

Figure 12. Tracking of transplanted medium and photoreceptor precursors by MRI. Longitudinal T2*WI of RCS rat eyes injected with SPION-labeled photoreceptor precursors (first row), SPION-containing medium (second row), unlabeled photoreceptor precursors (third row), and control medium (fourth row) at 1 day, 2 weeks, 4 weeks, 8 weeks, and 12 weeks after subretinal transplantation. One representative eye was selected for each group, and the injected sites are marked with white arrows.

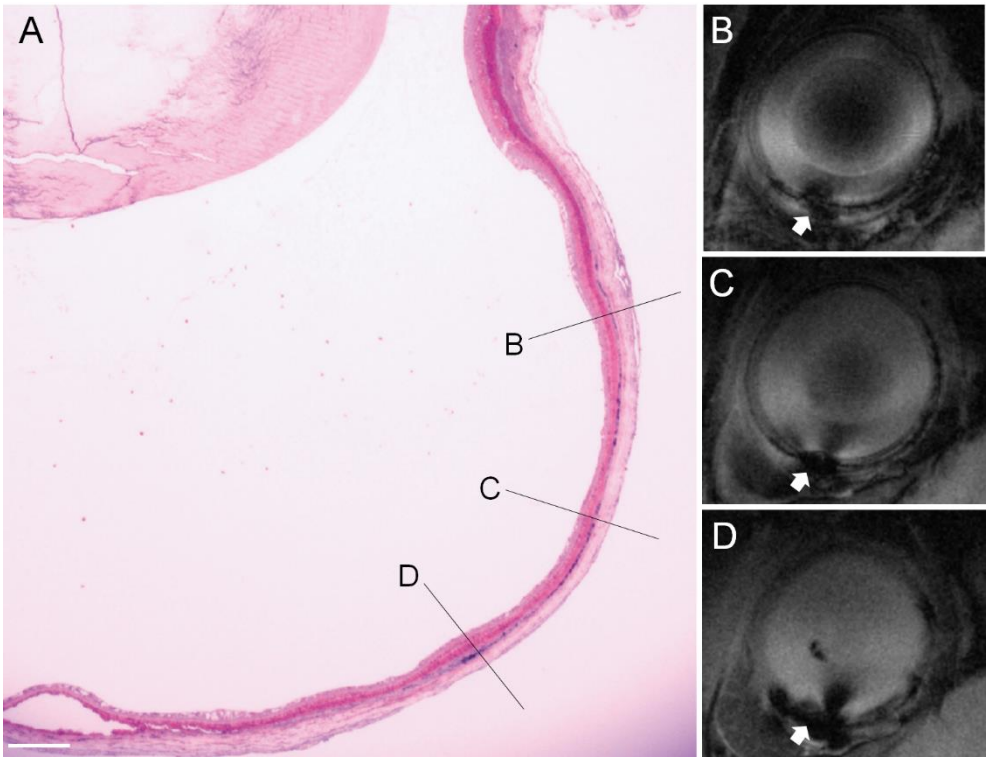

Figure 13. Histological analysis and MRI tracking of the transplanted SPION-labeled photoreceptor precursors. (A) Prussian blue staining. (B–D) T2*WI corresponding to each selected histological section plane. The injected sites are marked with white arrows (bar = 200 μm).

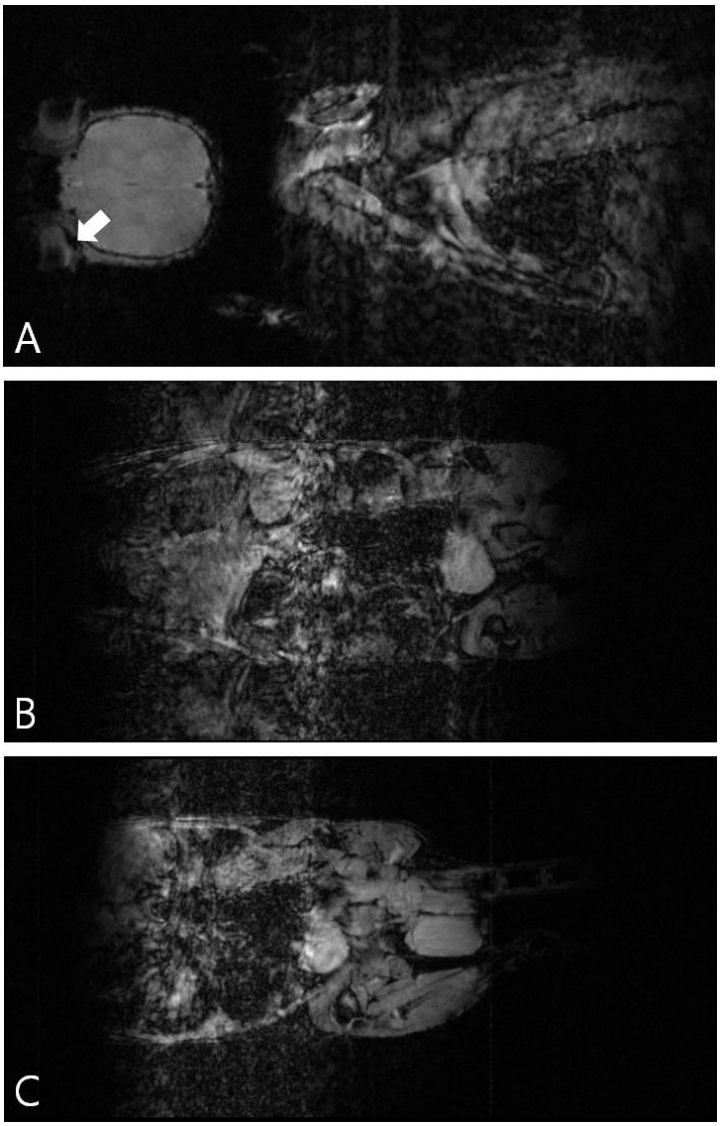

Figure 14. Whole body tracking of transplanted SPION-labeled photoreceptor precursors by MRI. Whole body T2*WI of RCS rats injected with SPION-labeled photoreceptor precursors. (A) Head and upper trunk. (B) Middle trunk. (C) Lower trunk. The injected sites are marked with white arrows.

Evaluation of in vivo *survival and localization of the SPION-labeled photoreceptor precursors by histological analysis*

To evaluate the survival and localization of the transplanted photoreceptor precursors, histological analysis was performed 1 week after transplantation. Prussian blue staining (Fig. 15A) and immunohistochemical staining (Fig. 15B) of SPION-labeled photoreceptor precursors showed distinct subretinal cell clumps that stained with Prussian blue, strongly expressed the photoreceptor-specific marker rhodopsin, and co-stained with anti-human mitochondria antibody.

At 12 weeks after transplantation, unlabeled and SPION-labeled photoreceptor precursors expressed rhodopsin and co-stained with the anti-human mitochondria antibody (Fig. 16A and 16B, respectively). Only SPION-labeled photoreceptor precursors were detected on T2*WI as a hypointense signal (Fig. 16D), with no detection at the transplantation site of the unlabeled photoreceptor precursors (Fig. 16C). At 12 weeks after transplantation, the proportion of the hypointense signal in T2*WI showed significant correlation with the distribution area of the SPION-labeled photoreceptor precursors observed in the histological sections ($r = 0.969$, $p = 0.031$).

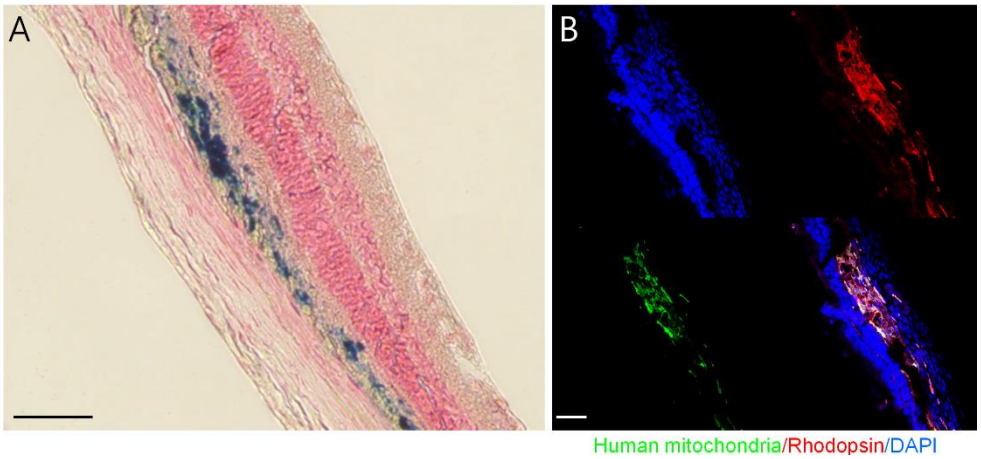

Figure 15. Histological analysis of the transplanted photoreceptor precursors at 1 week after transplantation. (A) Prussian blue staining for iron. (B) Immunostaining for rhodopsin, anti-human mitochondria, and DAPI (bar = 50 μm).

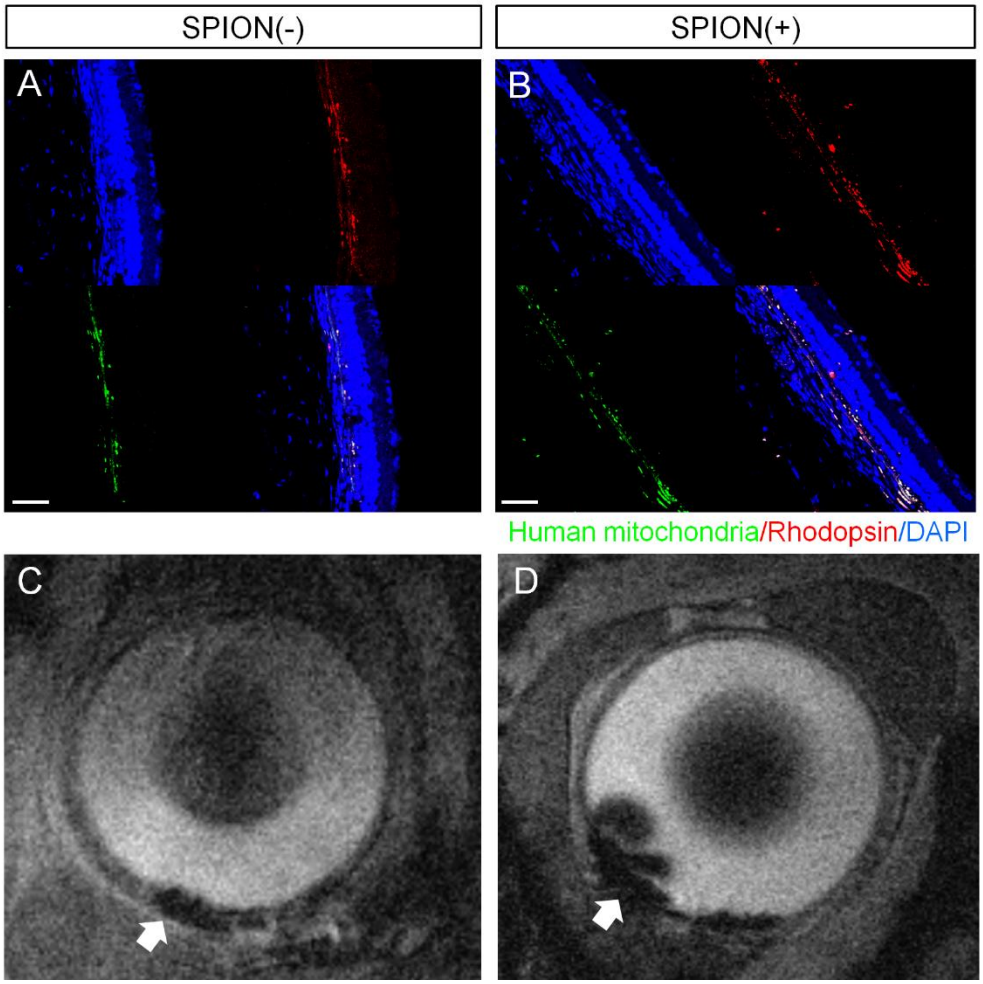

Figure 16. Immunostaining and MRI tracking of photoreceptor precursors at 12 weeks after transplantation. Immunostaining (unlabeled: A, SPION-labeled: B) and MRI (unlabeled: C, SPION-labeled: D) of the transplanted unlabeled and SPION-labeled photoreceptor precursors. The injected sites are marked with white arrows (bar = 50 μm).

Therapeutic effect of transplanted photoreceptor precursors

The functionality of the transplanted photoreceptor precursors was assessed via ERGs and OKRs at 2, 4, 8, and 12 weeks after transplantation. The findings showed that subretinal transplantation of photoreceptor precursors significantly delayed the reduction in the amplitudes of b-waves and the thresholds of OKR compared with those in the medium groups.

In ERGs, the b-wave amplitude in the medium group was significantly smaller than those in the unlabeled and SPION-labeled photoreceptor groups at 2 weeks (unlabeled: $p = 0.028$ and SPION-labeled: $p = 0.001$), 4 weeks (unlabeled: $p = 0.001$ and SPION-labeled: $p = 0.045$), and 8 weeks (unlabeled: $p = 0.011$ and SPION-labeled: $p = 0.002$) after transplantation. However, no significant difference was observed in the b-wave amplitude among groups at 12 weeks after transplantation (Fig. 17).

In OKRs, thresholds of OKR in the medium group was significantly smaller than those in the unlabeled and SPION-labeled photoreceptor groups at 2 weeks (unlabeled: $p = 0.036$ and SPION-labeled: $p = 0.003$) after transplantation. However, no significant difference was observed in the threshold of OKR among groups at 4, 8, and 12 weeks after transplantation (Fig. 18).

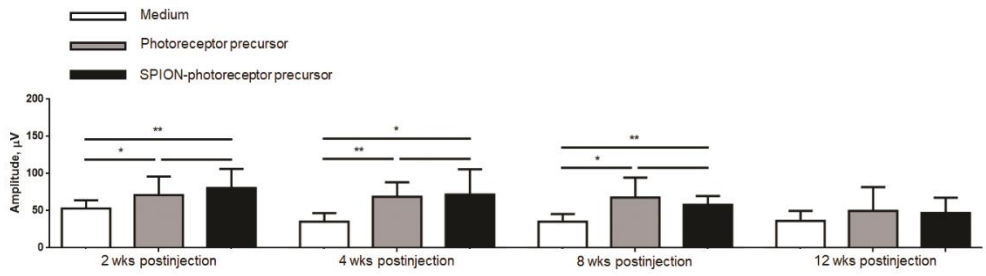

Figure 17. Comparison of ERG findings after photoreceptor precursor transplantation into the subretinal space. Statistical analysis of the amplitude of ERG b-wave in all three groups at four time-points; *$p < 0.05$; **$p < 0.01$. Error bars indicate standard deviations.

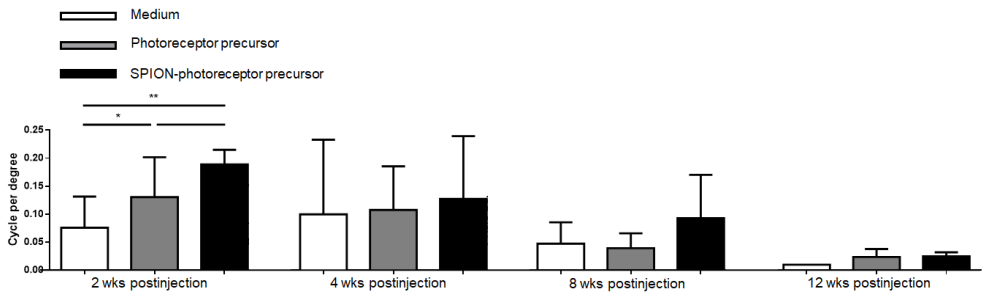

Figure 18. Comparison of OKR findings after photoreceptor precursor transplantation into the subretinal space. Statistical analysis of the threshold of OKR in all three groups at four time-points; *$p < 0.05$; **$p < 0.01$. Error bars indicate standard deviations.

DISCUSSION

Cell therapy might be a promising treatment strategy for the advanced stages of degenerative retinal diseases. Functional improvements after cell therapy with RPE cells, NP cells, photoreceptor precursors, and bone marrow-derived hematopoietic stem/progenitor cells have been observed in many preclinical studies and in a few clinical studies (4, 5, 15-17).

In subretinal transplantation, cell suspensions or sheets are injected into the subretinal space, creating a localized retinal bleb (18-21). Transplanted cells reside in the injection area in these approaches, and the therapeutic effect is limited to areas close to the transplantation site, which indicates that the biodistribution of the transplanted cells provides valuable information to assess the efficacy of cell therapy. Inaccurate localization during initial cell delivery is common, as one study reported that transplanted cells were inaccurately located in half of the cases even when transplantation was conducted by experienced operators under ultrasound guidance (22). The late detection of such conditions can seriously affect the outcome of the cell therapy. *In vivo* cellular imaging represents a noninvasive way to track transplanted cells; it can immediately detect the initial failure of cell delivery and evaluate the long-term efficacy of the treatment.

Only a few studies have evaluated the *in vivo* tracking of cells transplanted into the subretinal space. Lai et al. reported the tracking of green fluorescent protein

(GFP)-labeled RPE cells transplanted into the subretinal space by retroviral gene transfer (23). GFP-fluorescing cells were detected using infrared and fluorescence scanning laser ophthalmoscopy at 5 days after transplantation, but very few fluorescent cells were detected 2 weeks after transplantation. After 3–4 weeks, GFP fluorescence could not be detected in these transplants. Besides the short window for detection, GFP is antigenic, which might complicate long-term studies owing to the rejection of the transplants (24, 25). Recently, Mok et al. reported the detection of gold nanoparticle-labeled mesenchymal stem cells (MSCs) using micro-computed tomography (micro-CT) (26). The gold nanoparticle-labeled MSCs could be detected up to 1 month after transplantation in the subretinal space using micro-CT. However, micro-CT provides poor soft-tissue contrast, which severely limits the evaluation of the initial delivery accuracy, biodistribution, and therapeutic effect of the transplanted cells. In contrast, MRI provides high-resolution and three-dimensional stereoscopic viewing of the location of transplanted cells and surrounding tissues at the same time, as well as pathological changes such as inflammation and edema (27).

SPIONs are FDA-approved for use as an MRI contrast agent. Each SPION consists of a crystalline iron oxide core with a polymeric or polysaccharide coating to enhance solubility, biocompatibility, and bioavailability (28). SPIONs can form stable colloidal suspensions, which is crucial for *in vivo* biomedical applications (29). SPION-labeled cells appear as a dark signal on T2*WI, which enables the detection of the labeled cells with strong contrast and excellent depth penetration (30, 31). In

addition, the stability of SPIONs in the cellular milieu prevents their degradation over time and allows long-term tracking, suitable for longitudinal follow-up. Several studies have been performed using MRI tracking with SPION labeling to evaluate the effectiveness of cell therapy, namely, preclinical studies of various disease models such as stroke, spinal cord injury, multiple sclerosis, myocardial infarction, and arterial injury (31-37), as well as clinical studies on patients with brain trauma, multiple sclerosis, and amyotrophic lateral sclerosis (38, 39).

However, there are several limitations to *in vivo* cell tracking using SPION. First, the transplanted cells might replicate, divide, and exocytose SPIONs (40, 41), which might lead to the dilution of the intracellular SPION concentration as well as a decrease in the proportion of SPION-labeled cells. In the present study, the proportion of photoreceptor precursors stained with Prussian blue was decreased at 3 weeks after labeling, when compared with that at 1 day after labeling (Fig. 6C and 6D); however, the proportion of photoreceptor precursors stained with Prussian blue at the later period was not evaluated. The dilution of the intracellular SPION concentration and decrease in the proportion of SPION-labeled cells may lead to a weakened or distorted image, and may hinder an accurate quantification of the transplanted cells. Further studies evaluating the longitudinal change in the intracellular SPION concentration and the proportion of SPION-labeled cells are required.

Second, MRI tracking of SPION-labeled cells would be unable to

distinguish viable cell transplants from nonviable cell transplants (42). In addition, SPIONs from transplanted cells undergoing apoptosis or cell lysis could be engulfed by macrophages, which might be misinterpreted as SPION-labeled transplanted cells in T2*WI (42). To determine whether free SPIONs can be transferred to surrounding cells in the subretinal space including RPE or macrophages, we assessed the fate of SPION-containing medium *in vivo*. The hypointense signal from SPION-containing medium decreased markedly and was undetectable 12 weeks after transplantation, indicating that no significant iron label transfer had occurred in the subretinal space during the follow-up period. This is probably because the subretinal space is immune privileged, i.e., presumed to be free from macrophages. Therefore, further studies evaluating the fate of the free SPIONs in the subretinal space are required.

Dual labeling with GFP and SPION can be an effective method for overcoming these limitations of SPION. GFP expression is usually maintained after several passages (43), which may compensate the dilution of the intracellular SPION concentration and the decrease in the proportion of SPION-labeled cells. In addition, GFP and can be used as a marker for cell viability (44). An identical pattern of the GFP expression and the hypointensity signals in T2*WI indicates that the hypointensity signals are derived from the SPIO-labeled photoreceptor precursors, rather than macrophages. *In vivo* GFP expression can be observed in a transparent structure such as the retina, unlike other organs. The short window for GFP detection, as described above, can be compensated with the use of SPION. Further studies

evaluating the feasibility of dual labeling with GFP and SPION *in vivo* cell tracking after subretinal transplantation are required.

The eye is a suitable organ for MRI tracking with SPIONs using T2*WI, as there is no structure that produces a hypointense signal that might be confused with SPION labeling (45). In the present study, whole body MRI was conducted to evaluate the feasibility of SPION labeling and MRI tracking as a systemic distribution test of transplanted cells (Fig. 14). However, the hypointense signal of the SPION-labeled photoreceptor precursors was not distinguishable from the hypointense signal of the internal organs. In addition, rapid breathing of the rat caused severe motion artifacts in the body imaging.

In the present study, photoreceptor precursors incorporated SPIONs with high efficiency, showing homogeneous cytoplasmic distribution (Fig. 6). In addition, SPION labeling did not affect the proliferation, viability, or differentiation capacity of photoreceptor precursors (Figs. 7, 8, 9, 10, and 11). To our knowledge, this study is the first to demonstrate SPION labeling of photoreceptor precursors and evaluate the proliferation, viability, differentiation capacity, and therapeutic effect of SPION-labeled photoreceptor precursors. No adverse cellular effects of SPION labeling in different cell types, including human MSCs, human muscle precursor cells, and human neural stem cells, have been reported yet (3, 46-49). High nanoparticle loads are desirable from the imaging standpoint but could result in cytotoxicity (50). Herein, we found that a SPION concentration of 100 mg/mL displayed no cytotoxicity on

photoreceptor precursors and showed high signal alteration in T2*WI, sufficient for tracking (Figs. 12, 13 and 16).

SPION-labeled photoreceptor precursors transplanted into the subretinal space of RCS rats were observed as a hypointense signal in T2*WIs over 12 weeks (Fig. 12). This hypointense signal and its size corresponded to and correlated with the distribution of SPION-labeled photoreceptor precursors in histological sections (Fig. 13). Strong hypointense signals were observed as projections in the vitreous cavity (Figs. 12A, 13D, and 16D), which can be misinterpreted as the presence of SPION-labeled photoreceptor precursors in the vitreous cavity. However, in histological sections, transplanted cells were restricted only in the subretinal space, meaning that the hypointense signal extending into the vitreous cavity is an imaging artifact due to strong signal intensity.

Long-term *in vivo* cellular imaging methods for retinal cell therapy are clinically important because transplanted cells into the subretinal space can survive over 2 years, as demonstrated in a primate model (51). Ocular immune privilege may reduce rejection of transplanted cells (52), which may be advantageous for longer survival of retinal cell transplants.

Using RCS rats, a widely studied retinal degeneration model, we evaluated the efficacy of SPION-labeled photoreceptor precursors as cell therapy for degenerative retinal diseases, as well as the feasibility of SPION labeling and MRI tracking. This approach might shorten the timeline for clinical applications of SPION

labeling in cell therapy for degenerative retinal diseases. Both SPION-labeled photoreceptor precursors and unlabeled photoreceptor precursors delayed photoreceptor degeneration in RCS rats until 8 weeks after transplantation (Figs. 17 and 18), consistent with previous reports (53-56). There was no significant difference in the ERG b-wave amplitude and OKR threshold between unlabeled and SPION-labeled photoreceptor precursor recipients, which indicated that SPION labeling did not influence the rescue effect.

The present study had certain limitations in addition to the aforementioned limitations of SPIONs. First, the number of animals included was small. Further studies using larger sample sizes are required to confirm the effectiveness of SPION labeling and MRI tracking of photoreceptor precursors. Next, the precise quantification of SPIONs was not performed in the present study. The quantification of SPIONs is important because it aids in the monitoring and optimization of cellular therapies. We measured the size of hypointense signals in T2*WI and showed that it was correlated with the distribution area of the transplanted cells in histological sections. However, precise MRI-based quantification of SPIONs using relaxometry methods and model-based methods with special imaging protocols may be warranted (43). A future study involving an appropriate quantification method is expected to support the findings of the present study.

Our results suggest that photoreceptor precursors can be labeled with SPIONs and that the labeling does not affect the proliferation, viability, or

differentiation capacity of photoreceptor precursors. The SPION-labeled photoreceptor precursors were viable, with the expression of characteristic markers of photoreceptor cells *in vivo* for up to 12 weeks. Furthermore, the position of the transplanted cells could be visualized with T2*WI for up to 12 weeks. This study demonstrates the feasibility of SPION labeling of photoreceptor precursors and MRI tracking of SPION-labeled cells after subretinal transplantation. Thus, we present a novel noninvasive *in vivo* cellular imaging strategy that can improve the functional benefits of cell therapy in degenerative retinal diseases.

REFERENCES

1. Davis BM, Crawley L, Pahlitzsch M, Javaid F, Cordeiro MF. Glaucoma: the retina and beyond. Acta Neuropathol. 2016;132(6):807-26.

2. de Jong PT. Age-related macular degeneration. N Engl J Med. 2006;355(14):1474-85.

3. Francesco P, Francesco SS, Diego P, Vanessa B, Stefano F, Enzo Di I. Retinitis Pigmentosa: Genes and Disease Mechanisms. Current Genomics. 2011;12(4):238-49.

4. Schwartz SD, Regillo CD, Lam BL, Eliott D, Rosenfeld PJ, Gregori NZ, et al. Human embryonic stem cell-derived retinal pigment epithelium in patients with age-related macular degeneration and Stargardt's macular dystrophy: follow-up of two open-label phase 1/2 studies. Lancet. 2015;385(9967):509-16.

5. Mandai M, Watanabe A, Kurimoto Y, Hirami Y, Morinaga C, Daimon T, et al. Autologous Induced Stem-Cell-Derived Retinal Cells for Macular Degeneration. N Engl J Med. 2017;376(11):1038-46.

6. Shafiq M, Jung Y, Kim SH. Insight on stem cell preconditioning and instructive biomaterials to enhance cell adhesion, retention, and engraftment for tissue repair. Biomaterials. 2016;90:85-115.

7. Hyun JS, Tran MC, Wong VW, Chung MT, Lo DD, Montoro DT, et al. Enhancing stem cell survival in vivo for tissue repair. Biotechnol Adv. 2013;31(5):736-43.

8. Bulte JW. In vivo MRI cell tracking: clinical studies. AJR Am J Roentgenol.

2009;193(2):314-25.

9. Scholl HP, Strauss RW, Singh MS, Dalkara D, Roska B, Picaud S, et al. Emerging therapies for inherited retinal degeneration. Sci Transl Med. 2016;8(368):368rv6.

10. Park JH, Ku SY, Cho MS, Lee H, Choi YM, Moon SY, et al. Stem Cell Based Strategies for the Treatment of Degenerative Retinal Diseases. Korean Journal of Reproductive Medicine. 2010;37(3):199-206.

11. DiLoreto DA, Jr., Das T, del Cerro C, Cox C, del Cerro M. Fluorescein as a marker for subretinal transplantation of human fetal neural retina. Curr Eye Res. 1997;16(11):1159-65.

12. Cho MS, Hwang DY, Kim DW. Efficient derivation of functional dopaminergic neurons from human embryonic stem cells on a large scale. Nat Protoc. 2008;3(12):1888-94.

13. Wang S, Lu B, Wood P, Lund RD. Grafting of ARPE-19 and Schwann cells to the subretinal space in RCS rats. Invest Ophthalmol Vis Sci. 2005;46(7):2552-60.

14. Gasparini SJ, Llonch S, Borsch O, Ader M. Transplantation of photoreceptors into the degenerative retina: Current state and future perspectives. Prog Retin Eye Res. 2019;69:1-37.

15. Borsch O, Santos-Ferreira T, Ader M. [Photoreceptor Transplantation into the Degenerative Retina]. Klin Monbl Augenheilkd. 2017;234(3):343-53.

16. Tzameret A, Sher I, Belkin M, Treves AJ, Meir A, Nagler A, et al. Transplantation of human bone marrow mesenchymal stem cells as a thin subretinal layer ameliorates retinal degeneration in a rat model of retinal dystrophy. Exp Eye

Res. 2014;118:135-44.

17. Tsai Y, Lu B, Bakondi B, Girman S, Sahabian A, Sareen D, et al. Human iPSC-Derived Neural Progenitors Preserve Vision in an AMD-Like Model. Stem Cells. 2015;33(8):2537-49.

18. Gamm DM, Wang S, Lu B, Girman S, Holmes T, Bischoff N, et al. Protection of visual functions by human neural progenitors in a rat model of retinal disease. PLoS One. 2007;2(3):e338.

19. Wang S, Girman S, Lu B, Bischoff N, Holmes T, Shearer R, et al. Long-term vision rescue by human neural progenitors in a rat model of photoreceptor degeneration. Invest Ophthalmol Vis Sci. 2008;49(7):3201-6.

20. Idelson M, Alper R, Obolensky A, Ben-Shushan E, Hemo I, Yachimovich-Cohen N, et al. Directed differentiation of human embryonic stem cells into functional retinal pigment epithelium cells. Cell Stem Cell. 2009;5(4):396-408.

21. Lu B, Wang S, Girman S, McGill T, Ragaglia V, Lund R. Human adult bone marrow-derived somatic cells rescue vision in a rodent model of retinal degeneration. Exp Eye Res. 2010;91(3):449-55.

22. de Vries IJ, Lesterhuis WJ, Barentsz JO, Verdijk P, van Krieken JH, Boerman OC, et al. Magnetic resonance tracking of dendritic cells in melanoma patients for monitoring of cellular therapy. Nat Biotechnol. 2005;23(11):1407-13.

23. Lai CC, Gouras P, Doi K, Lu F, Kjeldbye H, Goff SP, et al. Tracking RPE transplants labeled by retroviral gene transfer with green fluorescent protein. Invest Ophthalmol Vis Sci. 1999;40(9):2141-6.

24. Stripecke R, Carmen Villacres M, Skelton D, Satake N, Halene S, Kohn D.

Immune response to green fluorescent protein: implications for gene therapy. Gene Ther. 1999;6(7):1305-12.

25. Rosenzweig M, Connole M, Glickman R, Yue SP, Noren B, DeMaria M, et al. Induction of cytotoxic T lymphocyte and antibody responses to enhanced green fluorescent protein following transplantation of transduced CD34(+) hematopoietic cells. Blood. 2001;97(7):1951-9.

26. Mok PL, Leow SN, Koh AE, Mohd Nizam HH, Ding SL, Luu C, et al. Micro-Computed Tomography Detection of Gold Nanoparticle-Labelled Mesenchymal Stem Cells in the Rat Subretinal Layer. Int J Mol Sci. 2017;18(2).

27. Anderson SA, Glod J, Arbab AS, Noel M, Ashari P, Fine HA, et al. Noninvasive MR imaging of magnetically labeled stem cells to directly identify neovasculature in a glioma model. Blood. 2005;105(1):420-5.

28. Wahajuddin, Arora S. Superparamagnetic iron oxide nanoparticles: magnetic nanoplatforms as drug carriers. International journal of nanomedicine. 2012;7:3445-71.

29. Wang YX, Idee JM. A comprehensive literatures update of clinical researches of superparamagnetic resonance iron oxide nanoparticles for magnetic resonance imaging. Quant Imaging Med Surg. 2017;7(1):88-122.

30. Long CM, Bulte JW. In vivo tracking of cellular therapeutics using magnetic resonance imaging. Expert Opin Biol Ther. 2009;9(3):293-306.

31. Ha BC, Jung J, Kwak BK. Susceptibility-weighted imaging for stem cell visualization in a rat photothrombotic cerebral infarction model. Acta Radiol. 2015;56(2):219-27.

32. Xu HS, Ma C, Cao L, Wang JJ, Fan XX. Study of co-transplantation of SPIO labeled bone marrow stromal stem cells and Schwann cells for treating traumatic brain injury in rats and in vivo tracing of magnetically labeled cells by MRI. Eur Rev Med Pharmacol Sci. 2014;18(4):520-5.

33. Song HT, Choi JS, Huh YM, Kim S, Jun YW, Suh JS, et al. Surface modulation of magnetic nanocrystals in the development of highly efficient magnetic resonance probes for intracellular labeling. J Am Chem Soc. 2005;127(28):9992-3.

34. Bulte JW, Ben-Hur T, Miller BR, Mizrachi-Kol R, Einstein O, Reinhartz E, et al. MR microscopy of magnetically labeled neurospheres transplanted into the Lewis EAE rat brain. Magn Reson Med. 2003;50(1):201-5.

35. Cohen ME, Muja N, Fainstein N, Bulte JW, Ben-Hur T. Conserved fate and function of ferumoxides-labeled neural precursor cells in vitro and in vivo. J Neurosci Res. 2010;88(5):936-44.

36. Kim D, Chun BG, Kim YK, Lee YH, Park CS, Jeon I, et al. In vivo tracking of human mesenchymal stem cells in experimental stroke. Cell Transplant. 2008;16(10):1007-12.

37. Gao F, Kar S, Zhang J, Qiu B, Walczak P, Larabi M, et al. MRI of intravenously injected bone marrow cells homing to the site of injured arteries. NMR Biomed. 2007;20(7):673-81.

38. Zhu J, Zhou L, XingWu F. Tracking neural stem cells in patients with brain trauma. N Engl J Med. 2006;355(22):2376-8.

39. Karussis D, Karageorgiou C, Vaknin-Dembinsky A, Gowda-Kurkalli B, Gomori JM, Kassis I, et al. Safety and immunological effects of mesenchymal stem

cell transplantation in patients with multiple sclerosis and amyotrophic lateral sclerosis. Arch Neurol. 2010;67(10):1187-94.

40. Guzman R, Uchida N, Bliss TM, He D, Christopherson KK, Stellwagen D, et al. Long-term monitoring of transplanted human neural stem cells in developmental and pathological contexts with MRI. Proc Natl Acad Sci U S A. 2007;104(24):10211-6.

41. Oh N, Park JH. Endocytosis and exocytosis of nanoparticles in mammalian cells. Int J Nanomedicine. 2014;9 Suppl 1:51-63.

42. Terrovitis J, Stuber M, Youssef A, Preece S, Leppo M, Kizana E, et al. Magnetic resonance imaging overestimates ferumoxide-labeled stem cell survival after transplantation in the heart. Circulation. 2008;117(12):1555-62.

43. Goodfellow F, Simchick GA, Mortensen LJ, Stice SL, Zhao Q. Tracking and Quantification of Magnetically Labeled Stem Cells using Magnetic Resonance Imaging. Adv Funct Mater. 2016;26(22):3899-915.

44. Li Y, Horwitz MS. Use of green fluorescent protein in studies of apoptosis of transfected cells. Biotechniques. 1997;23(6):1026-9.

45. Loebinger MR, Kyrtatos PG, Turmaine M, Price AN, Pankhurst Q, Lythgoe MF, et al. Magnetic resonance imaging of mesenchymal stem cells homing to pulmonary metastases using biocompatible magnetic nanoparticles. Cancer Res. 2009;69(23):8862-7.

46. Laffon B, Fernandez-Bertolez N, Costa C, Brandao F, Teixeira JP, Pasaro E, et al. Cellular and Molecular Toxicity of Iron Oxide Nanoparticles. Adv Exp Med Biol. 2018;1048:199-213.

47. Hsiao J-K, Tai M-F, Chu H-H, Chen S-T, Li H, Lai D-M, et al. Magnetic nanoparticle labeling of mesenchymal stem cells without transfection agent: Cellular behavior and capability of detection with clinical 1.5 T magnetic resonance at the single cell level. 2007;58(4):717-24.

48. Azzabi F, Rottmar M, Jovaisaite V, Rudin M, Sulser T, Boss A, et al. Viability, differentiation capacity, and detectability of super-paramagnetic iron oxide-labeled muscle precursor cells for magnetic-resonance imaging. Tissue engineering Part C, Methods. 2015;21(2):182-91.

49. Gutova M, Frank JA, D'Apuzzo M, Khankaldyyan V, Gilchrist MM, Annala AJ, et al. Magnetic resonance imaging tracking of ferumoxytol-labeled human neural stem cells: studies leading to clinical use. Stem Cells Transl Med. 2013;2(10):766-75.

50. Szalay B, Tatrai E, Nyiro G, Vezer T, Dura G. Potential toxic effects of iron oxide nanoparticles in in vivo and in vitro experiments. J Appl Toxicol. 2012;32(6):446-53.

51. Tu HY, Watanabe T, Shirai H, Yamasaki S, Kinoshita M, Matsushita K, et al. Medium- to long-term survival and functional examination of human iPSC-derived retinas in rat and primate models of retinal degeneration. EBioMedicine. 2019;39:562-74.

52. Bull ND, Martin KR. Concise review: toward stem cell-based therapies for retinal neurodegenerative diseases. Stem Cells. 2011;29(8):1170-5.

53. Lamba DA, Gust J, Reh TA. Transplantation of human embryonic stem cell-derived photoreceptors restores some visual function in Crx-deficient mice. Cell Stem Cell. 2009;4(1):73-9.

54. Singh MS, Charbel Issa P, Butler R, Martin C, Lipinski DM, Sekaran S, et al. Reversal of end-stage retinal degeneration and restoration of visual function by photoreceptor transplantation. Proc Natl Acad Sci U S A. 2013;110(3):1101-6.

55. Warre-Cornish K, Barber AC, Sowden JC, Ali RR, Pearson RA. Migration, integration and maturation of photoreceptor precursors following transplantation in the mouse retina. Stem Cells Dev. 2014;23(9):941-54.

56. Tucker BA, Park IH, Qi SD, Klassen HJ, Jiang C, Yao J, et al. Transplantation of adult mouse iPS cell-derived photoreceptor precursors restores retinal structure and function in degenerative mice. PLoS One. 2011;6(4):e18992.

국문 초록

생체 내 세포 추적은 세포치료의 최적화 및 모니터링을 위한 강력한 도구로 사용될 수 있다. 자기공명영상(magnetic resonance imaging, MRI)은 초자성 산화철 나노입자(superparamagnetic iron oxide nanoparticles, SPION)로 표지 한 세포 및 주변 조직의 시각화에 이용될 수 있으나, 망막하 이식에 대한 적용가능성은 아직 연구된 바 없다. 본 연구의 목적은 SPION 라벨링 및 MRI 추적이 망막하 공간 세포 이식에 적용이 가능한지를 평가하는 것이다. FeraTrack MRI 조영 키트를 이용하여 인간 배아줄기세포 유래 신경전구체 세포 및 광수용체 전구세포에 SPION을 라벨링하였다. Brown-Norway 랫트의 망막하 공간에 이식된 SPION 라벨링한 신경전구체 세포는 T2*강조 MRI (T2*WI)에서 이식 후 20주까지 저신호강도로 관찰이 되었다. 광수용체 전구세포에 대한 SPION 라벨링의 세포증식, 세포생존 및 세포분화에 대한 영향을 평가하였으며, 특별한 영향을 미치지 않은 것으로 관찰되었다. 21주령의 Royal College of Surgeons (RCS) 랫트를 세포배양 배지를 주입한 군, SPION 라벨링하지 않은 광수용체 전구세포를 주입한 군, SPION을 함유한 세포배양 배지를 주입한 군, 그리고 SPION 라벨링한 광수용체 전구세포를 주입한 군, 총 4개의 실험군으로 분류되었다. 모든 RCS 랫트는 경공막접근법을 통하여 망막하 이식을 시행하였으며, T2*WI를 이용하여 이식 후 1일부터

12주까지 평가하였다. 이식 다음날 촬영한 T2*WI에서 이식된 SPION 라벨링한 광수용체 전구세포 및 SPION 함유 배지에 해당하는 저신호강도가 선명하게 관찰되었다. 반면 세포배양 배지 또는 SPION 라벨링하지 않은 광수용체 전구세포를 주입한 랫트에서는 저신호강도가 관찰되지 않았다. 이후 SPION 라벨링한 광수용체 전구세포의 저신호강도는 시간의 경과에 따라 감소하였으나, 연구 종료 시점까지 관찰이 가능하였다. 이식 12주 후 시행한 조직검사에서 망막하 공간에 이식된 SPION 라벨링한 광수용체 전구세포가 생존함이 관찰되었으며, 이들의 분포는 T2*WI에서 관측된 저신호강도와 일치하였다. 반면 SPION을 함유한 세포배양 배지의 저신호강도는 시간의 경과에 따라 감소하여, 이식 12주 후에는 관찰되지 않았다. 또한, SPION 라벨링한 광수용체는 SPION 라벨링하지 않은 광수용체 전구세포와 비슷한 정도의 RCS 랫트의 망막변성 지연효과를 보였다. 본 연구 결과 SPION 라벨링과 MRI 추적은 망막하 공간의 세포 이식에 적용이 가능하며, 망막변성질환의 세포치료에 활용할 수 있을 것으로 기대된다.

……

Keywords: 망막, 인간 배아줄기세포, 초자성 산화철 나노입자, 광수용체 전구세포, 자기공명영상

학번: 2017-37618

* 본 졸업 논문의 일부는 현재 Tissue Engineering Part C: Methods (Ma DJ, Lim MS, Park UC, Park JB, Ji SY, Yu HG. Magnetic Iron Oxide Nanoparticle Labeling of Photoreceptor Precursors for Magnetic Resonance Imaging. 2019 Sep;25(9):532-542.)에 출판 완료된 내용을 포함하고 있습니다.

* This work was supported by the Bio & Medical Technology Development Program of the National Research Foundation of Korea (NRF) funded by the Korean Ministry of Science, ICT & Future Planning (grant number: NRF2015M3A9B4067004), and the Korea Health Technology R&D project of the Korea Health Industry Development Institute funded by the Korean Ministry of Health and Welfare (grant number: HI14C1277).